Allosteric PI3Kα Inhibition Overcomes On-target Resistance to Orthosteric Inhibitors Mediated by Secondary *PIK3CA* Mutations

Andreas Varkaris[1], Ferran Fece de la Cruz[1], Elizabeth E. Martin[2], Bryanna L. Norden[1], Nicholas Chevalier[1], Allison M. Kehlmann[1], Ignaty Leshchiner[3], Haley Barnes[1], Sara Ehnstrom[1], Anastasia-Maria Stavridi[4], Xin Yuan[4], Janice S. Kim[1], Haley Ellis[1], Alkistis Papatheodoridi[5], Hakan Gunaydin[6], Brian P. Danysh[7], Laxmi Parida[8], Ioannis Sanidas[1], Yongli Ji[9], Kayao Lau[1], Gerburg M. Wulf[4], Aditya Bardia[1], Laura M. Spring[1], Steven J. Isakoff[1], Jochen K. Lennerz[10], Kathryn Del Vecchio[6], Levi Pierce[6], Ermira Pazolli[6], Gad Getz[1,2,10], Ryan B. Corcoran[1], and Dejan Juric[1]

ABSTRACT

PIK3CA mutations occur in ~8% of cancers, including ~40% of HR-positive breast cancers, where the PI3K-alpha (PI3Kα)-selective inhibitor alpelisib is FDA approved in combination with fulvestrant. Although prior studies have identified resistance mechanisms, such as *PTEN* loss, clinically acquired resistance to PI3Kα inhibitors remains poorly understood. Through serial liquid biopsies and rapid autopsies in 39 patients with advanced breast cancer developing acquired resistance to PI3Kα inhibitors, we observe that 50% of patients acquire genomic alterations within the PI3K pathway, including *PTEN* loss and activating *AKT1* mutations. Notably, although secondary *PIK3CA* mutations were previously reported to increase sensitivity to PI3Kα inhibitors, we identified emergent secondary resistance mutations in *PIK3CA* that alter the inhibitor binding pocket. Some mutations had differential effects on PI3Kα-selective versus pan-PI3K inhibitors, but resistance induced by all mutations could be overcome by the novel allosteric pan-mutant-selective PI3Kα-inhibitor RLY-2608. Together, these findings provide insights to guide strategies to overcome resistance in *PIK3CA*-mutated cancers.

SIGNIFICANCE: In one of the largest patient cohorts analyzed to date, this study defines the clinical landscape of acquired resistance to PI3Kα inhibitors. Genomic alterations within the PI3K pathway represent a major mode of resistance and identify a novel class of secondary *PIK3CA* resistance mutations that can be overcome by an allosteric PI3Kα inhibitor.

See related commentary by Gong and Vanhaesebroeck, p. 204.

See related article by Varkaris et al., p. 240.

[1]Mass General Cancer Center and Department of Medicine, Harvard Medical School, Boston, Massachusetts. [2]Broad Institute of MIT and Harvard, Cambridge, Massachusetts. [3]Department of Medicine, Boston University, Boston, Massachusetts. [4]Department of Medicine, Beth Israel Deaconess Medical Center, Boston, Massachusetts. [5]National and Kapodistrian University of Athens, Athens, Greece. [6]Relay Therapeutics, Cambridge, Massachusetts. [7]Cancer Program, Broad Institute of MIT and Harvard, Cambridge, Massachusetts. [8]IBM Research, Yorktown Heights, New York. [9]Hematology-Oncology, Exeter Hospital, New Haven. [10]Department of Pathology, Massachusetts General Hospital, Boston, Massachusetts.

A. Varkaris, F.F. de la Cruz, and E.E. Martin contributed equally to this article.

Corresponding Authors: Dejan Juric, Mass General Cancer Center, 55 Fruit St., Boston, MA 02014. E-mail: juric.dejan@mgh.harvard.edu; and Ryan B. Corcoran, Mass General Cancer Center, 149 13th St., 7th Floor, Boston, MA 02129. E-mail: rbcorcoran@partners.org

Cancer Discov 2024;14:227–39

doi: 10.1158/2159-8290.CD-23-0704

INTRODUCTION

Activating mutations in *PIK3CA*, the gene encoding phosphoinositide-(3)-kinase α (PI3Kα), occur in 40% of advanced hormone receptor (HR)-positive, human epidermal growth factor receptor 2 (HER2)-negative breast cancers. Alpelisib, an orthosteric PI3Kα inhibitor, is FDA approved in this patient population in combination with fulvestrant, an estrogen receptor degrader (1). The therapeutic effect of alpelisib is limited by the narrow therapeutic index of this agent and by activation of multiple context-dependent resistance mechanisms, including *PTEN* loss, upstream receptor tyrosine kinase activation (AXL, IGF1R, FGFR), systemic glucose–insulin feedback, and downstream PI3K and MAPK pathway molecular effects (RSK3/4, FOXM1, PDK1-SGK1, GSK3; refs. 2–6). Many of these resistance drivers have been explored in the nonclinical setting, and their clinical impact remains to be characterized.

Here, we have integrated circulating tumor DNA (ctDNA) in serially collected plasma samples and molecular profiling studies of rapid autopsy tissue series from patients with *PIK3CA*-mutated $HR^+/HER2^-$ advanced breast cancer treated with alpelisib or inavolisib (a next-generation orthosteric PI3Kα inhibitor in late stages of drug development, also known as GDC-0077), to examine the on-target and off-target mechanisms of resistance to these agents and develop novel treatment sequencing strategies. We identify the emergence of secondary *PIK3CA* mutations within the catalytic pocket as a novel mechanism of resistance to orthosteric PI3Kα inhibitors. Through structural and *in vitro* modeling, we demonstrate that alterations affecting the Gln859 residue prevent the binding of orthosteric PI3Kα inhibitors, but not pan-PI3K inhibitors. Conversely, alterations at the critical Trp780 residue drive resistance to both PI3Kα and pan-PI3K inhibitors. We also show that a novel allosteric PI3Kα inhibitor RLY-2608 overcomes both types of on-target resistance mechanisms. However, co-occurring emergent *AKT1* mutations were also identified, representing an additional vulnerability resulting in cross-resistance to both orthosteric and allosteric PI3Kα inhibitors, reversed only with AKT inhibitors.

RESULTS

Acquired Resistance Alterations in Serial ctDNA from Patients Treated with Alpelisib and Inavolisib

To identify on-target and off-target alterations potentially mediating resistance to PI3Kα inhibitors, we used a targeted next-generation sequencing assay (Guardant360; Guardant Health) to analyze ctDNA in serially collected plasma samples from 32 patients with *PIK3CA*-mutated advanced HR-positive, HER2-negative breast cancer treated with alpelisib and inavolisib (Supplementary Table S1). Alterations considered within the PI3K pathway are shown in Supplementary Table S2. Of those, 20 received inavolisib and 12 received alpelisib. Acquired, end-of-treatment (EOT) genomic alterations within the PI3K pathway were observed in 50% of patients (Fig. 1A; Supplementary Table S3). Specifically, secondary *PIK3CA* mutations beyond the primary pretreatment *PIK3CA* mutation [$n = 9/32$ (28%)], as well as loss-of-function *PTEN* alterations [$n = 5/32$ (15%)] and activating *AKT1* [$n = 5/32$ (15%) alterations were detected. In *PTEN*-mutant tumors with available tissue, *PTEN* loss was confirmed with IHC (Supplementary Fig. S1). Because tissue was not available for all patients, the frequency of *PTEN* loss may be underrepresented in this study. More than one alteration was observed in 9% ($n = 3/32$) of cases [*PIK3CA* plus *AKT1* ($n = 1/32$) and *PIK3CA* plus *PTEN* ($n = 2/32$)]. Concomitant acquired alterations in *PTEN* and *AKT1* were not observed (Fig. 1B). Notably, mutations in 4 amino acid residues of *AKT1*—E17, L52, Q79, and D323—were identified, all of which have previously been confirmed to activate AKT kinase activity. Figure 1C and D shows the distribution of acquired on-target genomic alterations in inavolisib- and alpelisib-treated patients, respectively. There was a trend toward more frequent acquired *PIK3CA* mutations in alpelisib-treated patients ($P = 0.44$). Development of acquired PI3K genomic alterations was not influenced by primary *PIK3CA* alteration (kinase vs. helical vs. other) and the presence of double-*PIK3CA* mutants at baseline (Supplementary Table S4 and S5). Emerging alterations affecting upstream RTKs FGFR1 and FGFR2, as well as MAPK pathway mutations (*KRAS* and *BRAF*), were also detected.

Landscape of Acquired PI3K Alterations in Rapid Autopsy Tissue Series

To determine the spatial distribution of acquired PI3K genomic alterations, we performed whole-exome sequencing (WES) of 100 tissue samples collected from 8 autopsy series from patients with metastatic, *PIK3CA*-mutant HR-positive, HER2-negative breast cancer previously treated with PI3Kα inhibitors. Rapid autopsies were performed within a median of 6 hours after death. Acquired genomic alterations within the PI3K pathway were observed in 38% ($n = 3/8$) of analyzed cases (Fig. 2A). Specifically, acquired *PIK3CA* [$n = 3/8$ (38%)], *PTEN* [$n = 1/8$ (13%)], and *AKT1* [$n = 1/8$ (13%) alterations were detected. Notably, we observed more than one alteration in 2/8 (25%) of cases [*PIK3CA* plus *PTEN* ($n = 1/8$) and *PIK3CA* plus *AKT1* ($n = 1/8$). Concomitant acquired alterations in *PTEN* and *AKT1* were not observed (Fig. 2B). No clear acquired alterations in PIK3CB and PIK3CD were noted. The complete characterization of baseline and acquired on-target PI3K pathway genomic alterations are shown in Fig. 2C.

Next, we focused on a patient with multiple acquired alterations with convergent PI3K/AKT reactivation (autopsy ID: MGH2542). A 72-year-old female with metastatic *PIK3CA* H1047R, ER-positive, PR-negative, HER2-negative breast cancer was treated with inavolisib 9 mg daily (protocol

Figure 1. Acquired resistance alterations in serial ctDNA from patients treated with alpelisib and inavolisib. **A,** Incidence of acquired PI3K pathway genomic alterations in 42 patients with *PIK3CA*-mutant breast cancer treated with orthosteric *PIK3CA* inhibitors (left, total number; right, breakdown based on mutation type). **B,** Incidence and correlation of acquired *PIK3CA*, *PTEN*, and *AKT1* alterations in patients treated with inavolisib and alpelisib, respectively. **C** and **D,** Combination partners, response duration, baseline and emerging genomic in-pathway and bypassing pathway alterations of patients treated with inavolisib and alpelisib, respectively. FSM, frameshift mutation; PM, point mutation.

A

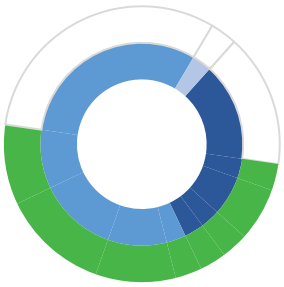

Baseline *PIK3CA* **kinase/helical** domain mutation
Total acquired PI3K pathway alterations

Acquired alterations
PIK3CA*, *PTEN*, *AKT1

B

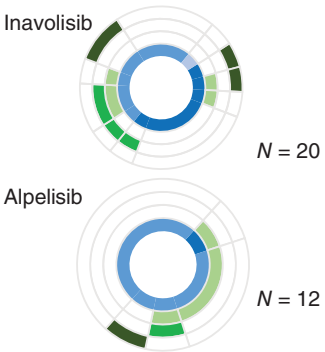

C

ID	Combo-partners			DOT	Baseline and acquired genomic alteration on inavolisib																												
					Baseline *PIK3CA*										Acquired *PIK3CA*							*PTEN*		*AKT1*				*CCND1*	*FGFR1*	*FGFR2*	*EGFR*	*RAS/RAF*	
								Double mutants																									
	CDK4/6 inh	Fulvestrant	Letrozole		Kinase	Helical	C2	E78K	N107I	N345K	D350N	E726K	E737Q	E970K	E172Q	E418K	S576C	W780R	Q859K	Q859H	M1004I	Ampl	Fsm/NM	Pm	E17K	L52R	Q79K	D323Y					*KRAS*	*BRAF*
1			■	1,620	■																												
2		■		896	■				■									■	■	■				■	■	■							
3		■		350	■																			■				■					
4		■		336	■																	■											
5		■		122	■															■													
6		■		182		■																						■					
7			■	1,367	■																									■		■	
8			■	182		■						■												■									
9			■	675		■						■				■						■							■				
10			■	783		■																■						■					
11				543	■																												
12		■		461		■																■					■						
13			■	476		■																											
14				232	■																												
15			■	195		■								■								■	■	■					■			■	
16			■	125		■		■				■			■							■		■								■	■
17			■	202	■						■																		■				
18			■	55		■																							■				
19				280		■						■				■							■	■									■
20				287			■			■																				■			

D

ID	Combo-Partners			DOT	Baseline and acquired genomic alteration on alpelisib																												
					Baseline *PIK3CA*										Acquired *PIK3CA*							*PTEN*		*AKT1*				*CCND1*	*FGFR1*	*FGFR2*	*EGFR2*	*RAS/RAF*	
								Double mutants																									
	CDK4/6 inh	Fulvestrant	Letrozole		Kinase	Helical	C2	E726K	I817F	R88Q	I197K	E453K	D549N	D725G	Ampl	Fsm/NM	Pm	E17K	L52R	D323Y										*KRAS*	*BRAF*
1		■		158	■			■		■																							
2		■		357		■					■																						
3	■		■	519		■												■														
4		■		85		■						■					■						■		■							
5	■		■	250		■			■																■							
6				214		■							■																				
7		■		142		■								■												■						
8				2,485*		■																											
9			■	1,922*		■																											
10			■	1,008		■								■																			
11				193		■																											
12			■	1,106		■																											

CDK4/6 inhibitor
Fulvestrant
Letrozole

PIK3CA kinase mutation
PIK3CA helical mutation
PIK3CA C2 mutation
Acquired mutation
Amplification

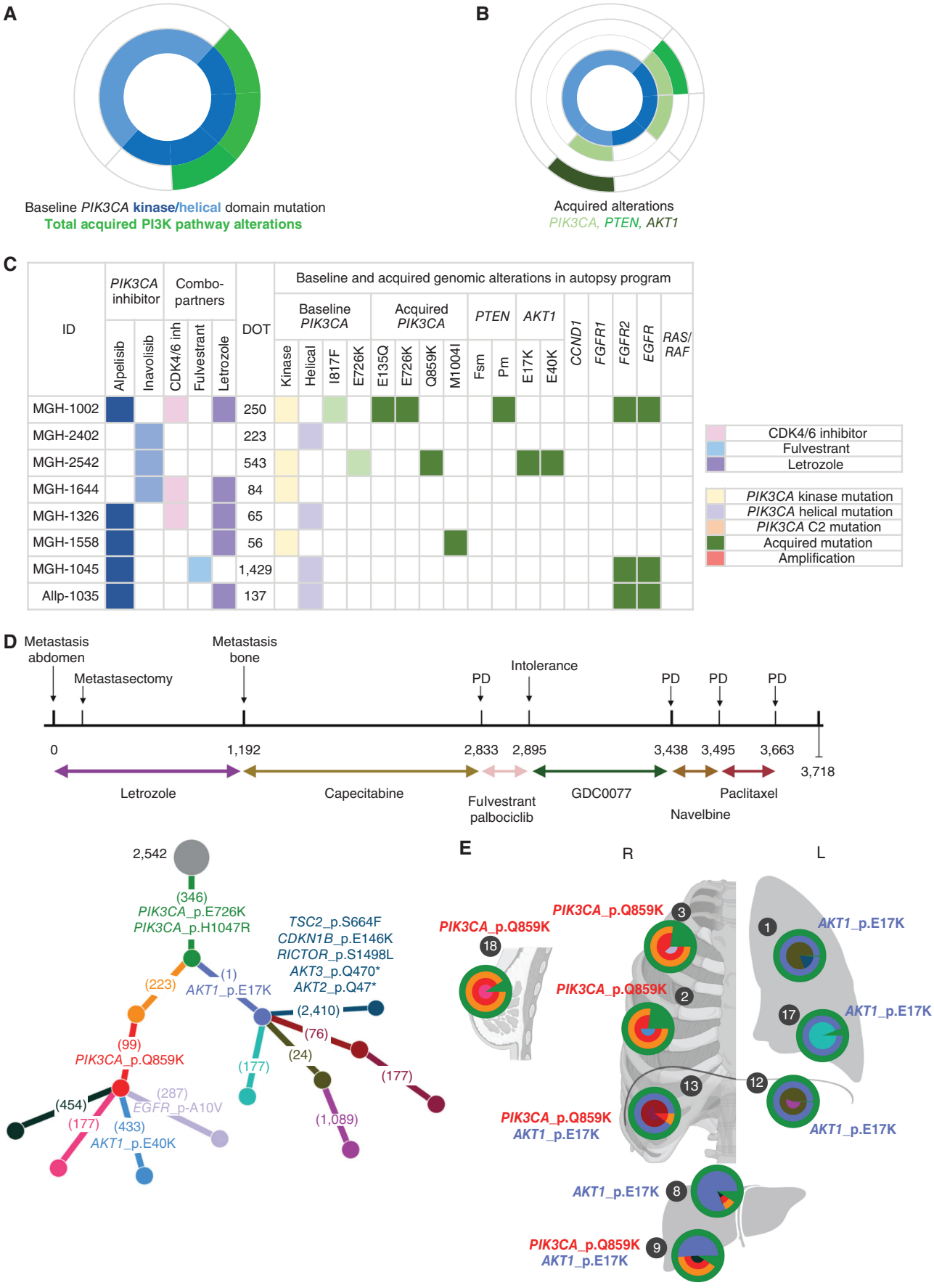
A
Baseline PIK3CA kinase/helical domain mutation
Total acquired PI3K pathway alterations
B
Acquired alterations
PIK3CA, PTEN, AKT1
C
ID
PIK3CA inhibitor
Alpelisib
Inavolisib
Combo-partners
CDK4/6 inh
Fulvestrant
Letrozole
DOT
Baseline and acquired genomic alterations in autopsy program
Baseline PIK3CA
Kinase
Helical
I817F
E726K
Acquired PIK3CA
E135Q
E726K
Q859K
M1004I
PTEN
Fsm
Pm
AKT1
E17K
E40K
CCND1
FGFR1
FGFR2
EGFR
RAS/RAF
MGH-1002 250
MGH-2402 223
MGH-2542 543
MGH-1644 84
MGH-1326 65
MGH-1558 56
MGH-1045 1,429
Allp-1035 137
CDK4/6 inhibitor
Fulvestrant
Letrozole
PIK3CA kinase mutation
PIK3CA helical mutation
PIK3CA C2 mutation
Acquired mutation
Amplification
D
Metastasis abdomen
Metastasectomy
Metastasis bone
PD
Intolerance
PD
PD
PD
0
1,192
2,833
2,895
3,438
3,495
3,663
3,718
Letrozole
Capecitabine
Fulvestrant
palbociclib
GDC0077
Paclitaxel
Navelbine
2,542
(346)
PIK3CA_p.E726K
PIK3CA_p.H1047R
TSC2_p.S664F
CDKN1B_p.E146K
RICTOR_p.S1498L
AKT3_p.Q470*
AKT2_p.Q47*
(223)
(1)
AKT1_p.E17K
(2,410)
(76)
(24)
(177)
(177)
(1,089)
(99)
PIK3CA_p.Q859K
(454)
(287)
EGFR_p-A10V
(177)
(433)
AKT1_p.E40K
E
R
L
PIK3CA_p.Q859K
18
PIK3CA_p.Q859K
3
PIK3CA_p.Q859K
2
PIK3CA_p.Q859K
AKT1_p.E17K
13
AKT1_p.E17K
8
PIK3CA_p.Q859K
AKT1_p.E17K
9
1
AKT1_p.E17K
17
AKT1_p.E17K
12
AKT1_p.E17K

NCT03006172). Initial on-treatment scans showed unchanged sclerotic and lytic osseous lesions with no evidence of new metastatic disease. After 543 days of treatment, she discontinued therapy due to the clinical progression of the disease. The patient was subsequently treated with vinorelbine monotherapy and paclitaxel monotherapy without any evidence of clinical, radiographic, or laboratory response to either agent and succumbed from her disease 9 months after discontinuing inavolisib. Complete treatment history is shown in Fig. 2D. The patient underwent autopsy within 8 hours of death. To identify putative mechanisms of acquired resistance to inavolisib, we performed WES in tissue samples collected at baseline and at autopsy. Phylogenic tree analysis demonstrated truncal *PIK3CA* H1047R and *PIK3CA* E726K alterations. Subclonal *AKT1* E17K and *PIK3CA* Q859K alterations were also observed. The distribution of *PIK3CA* Q859K and *AKT1* E17K alterations across collected autopsy tissue samples is shown in Fig. 2E. Notably, *PIK3CA* Q859K and *AKT1* E17K alterations are mutually exclusive in the majority of analyzed tumor samples. Lesions 9 and 13 show the presence of both mutations, but phylogenic analysis showed that these alterations were present in distinct clones (Fig. 2D and E). Despite mutual exclusivity between *PIK3CA* Q859K and *AKT1* E17K, *PIK3CA* Q859K-positive subclone acquired *AKT1* E40K mutation, suggesting that sequential acquisition of this minor *AKT1* mutation in the context of secondary *PIK3CA* mutation may provide further selective advantage (lesion 2; Fig. 2E).

De Novo Mutations in the PI3K/AKT Pathway Emerge during Treatment and Lead to Acquired Resistance

As described above, analysis of EOT clinical ctDNA assays and autopsy samples WES indicated heterogeneous mechanisms of resistance to orthosteric PI3Kα inhibitors. To better understand the clonal dynamics of resistance, we assessed serial ctDNA from two patients who developed acquired *PIK3CA* and *AKT1* mutations at progression to inavolisib. For this analysis, we used droplet digital PCR (ddPCR). Notably, both patients experienced clinical and laboratory response to therapy that was associated with complete clearance of the clonal *PIK3CA* H1047R mutation. The *PIK3CA* H1047R mutation became detectable again within 200–500 treatment days and preceded radiographic progression by approximately 300 days. The increase in *PIK3CA* H1047R variant allele frequency was accompanied by the emergence of other resistance alterations as shown in Fig. 3A and B. In patient 2542, we observed the emergence of a *PIK3CA* Q859K mutation as well as an *AKT1* E17K mutation accompanying the rise in detectable *PIK3CA* H1047R founder mutation (Fig. 3A). These mutations remained detectable after radiographic progression and up until the time of rapid autopsy (as shown in Figs. 2D and 3A). In patient 4643 (Fig. 3B), the rebound in *PIK3CA* H1047R mutation in ctDNA is accompanied by the emergence of the same *PIK3CA* Q859K mutation observed in patient 2542, but also by a plethora of alterations within the PI3K pathway, including a *PIK3CA* W780R mutation, as well as three mutations in *AKT1* (E17K, L52R, and Q79K). Notably, all three mutations in *AKT1* have previously been described to have oncogenic potential and result in activation of *AKT1* kinase activity (7, 8).

To further examine the role of *AKT1*-activating mutations to drive resistance to PI3Kα orthosteric inhibitors, we engineered the T47D (*PIK3CA*^{H1047R} mutant) breast cancer cell line to express *AKT1* E17K or Q79K constructs. In cell viability assays, cells expressing *AKT1* E17K or Q79K showed an increase in IC_{50} for alpelisib and inavolisib relative to controls expressing *AKT1* WT (Fig. 3C; Supplementary Figs. S2A and S2B, S3). In contrast, the effect of ipatasertib (an ATP-competitive pan-AKT inhibitor) was not affected by the expression of *AKT1* E17K or Q79K, suggesting that AKT inhibitors represent a potential therapeutic option for patients developing acquired resistance through activating AKT alterations.

Mutations in *PIK3CA* Involving Trp780 or Gln859 Impair the Activity of ATP-Competitive, Alpha-Selective PI3K Inhibitors

To examine the role of emergent secondary *PIK3CA* mutations observed in our patient cohort as potential acquired resistance mechanisms, we aimed to prioritize those secondary mutations most likely to promote acquired resistance to PI3Kα orthosteric inhibitors through a combination of structural modeling and free energy perturbation simulation (Fig. 4A and B; Supplementary Figs. S4 and S5). Notably, we found that two of the amino acids altered in emerging *PIK3CA* mutations—W780 and Q859—make direct contact with PI3Kα orthosteric inhibitors, and a third altered residue, I817, is in close proximity to the binding pocket. The catalytic subunit of PI3K (p110) is composed of four isoforms (α, β, δ, or γ; ref. 9), which harbor a high degree of amino acid sequence conservation around the ATP binding site, where catalytic small-molecule PI3K inhibitors bind (10). Interestingly, W780 is conserved in all PI3K isoforms, whereas Q859 is only present in PI3Kα (Fig. 4A). In fact, Q859 forms dual reciprocal hydrogen bonds with the amide group present in PI3Kα-selective orthosteric inhibitors such as alpelisib and inavolisib (Fig. 4B; Supplementary Fig. S5A), and this interaction is one of the key drivers of PI3Kα selectivity for

Figure 2. Acquired PI3K alterations in rapid autopsy tissue series of patients treated with orthosteric *PIK3CA* inhibitors. **A,** Incidence of acquired PI3K pathway genomic alterations in 8 patients with *PIK3CA* mutant breast cancer treated with orthosteric *PIK3CA* inhibitors. **B,** Incidence and correlation of acquired *PIK3CA*, *PTEN*, and *AKT1* alterations in patients treated with inavolisib and alpelisib, respectively. **C,** Combination partners, response duration, baseline, and emerging genomic in-pathway and bypassing pathway alterations of patients treated with inavolisib and alpelisib. **D,** Clinical history and phylogenic tree analysis of autopsy case from a patient with multiple acquired alterations with convergent PI3K/AKT reactivation (MGH2542). Numbers in parentheses represent the total number of alterations in each cluster. **E,** Distribution of *PIK3CA* Q859K and *AKT1* E17K alterations across collected autopsy tissue samples from autopsy case MGH2542 (lesion 1: L lung parenchyma; lesion 2: R chest wall; lesion 3: R mediastinum; lesion 8: R liver lobe (superior); lesion 9: R liver lobe (inferior); lesion 12: upper mesentery; lesion 13: diaphragm; lesion 17: L Lung parenchyma; lesion 18: right breast). Layered pie charts represent the likely clonal composition of each specimen, with the color of each subclone matching the color of the respective branch in the phylogenetic tree.

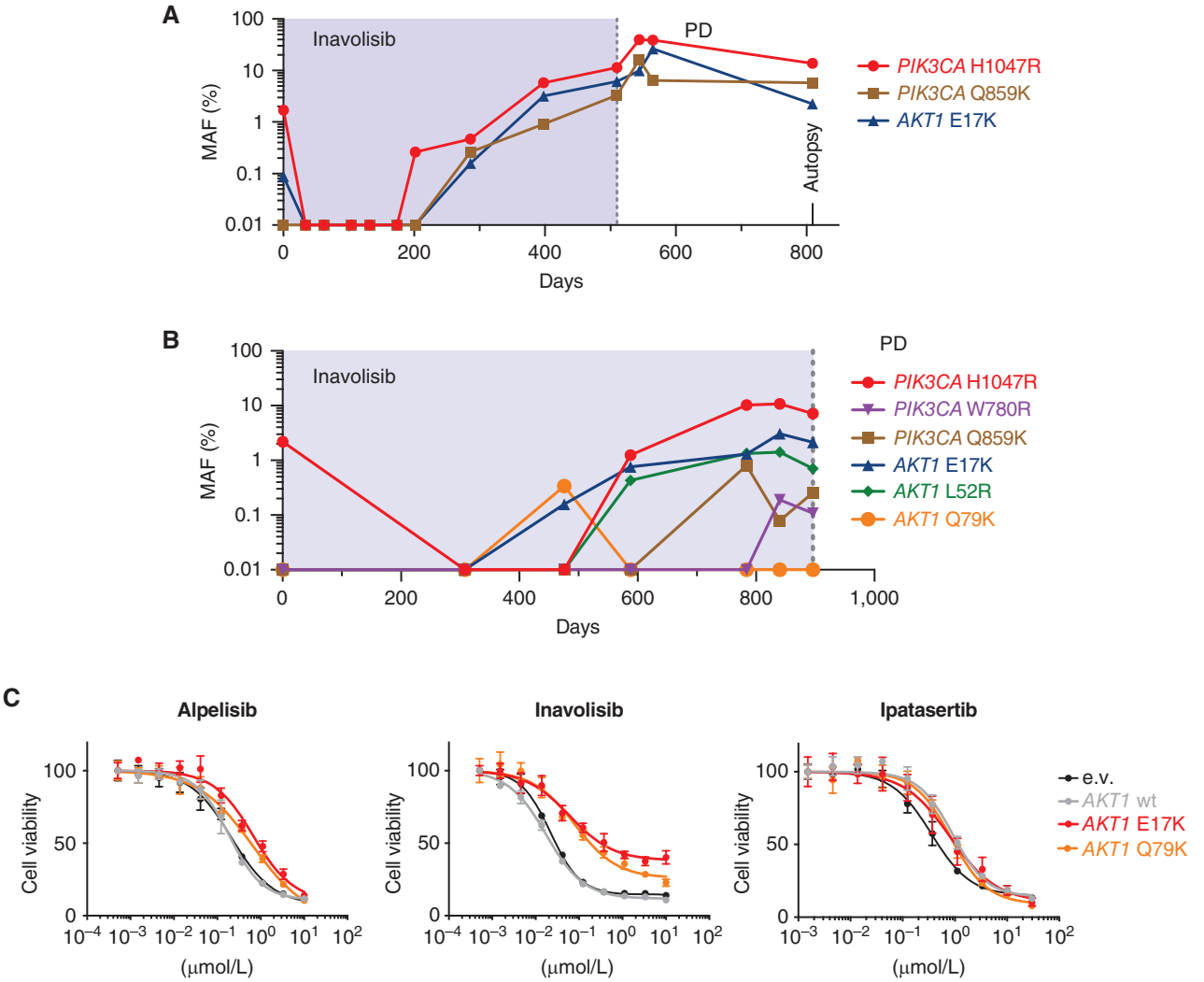

Figure 3. Secondary mutations in the PI3K/AKT pathway emerge during treatment with inavolisib and lead to acquired resistance. **A** and **B,** ddPCR analysis of serial ctDNA samples from patients 2542 and 4643. Treatment times with inavolisib are indicated by shading. **C,** Cell viability of T47D cells stably infected with the indicated *AKT1* expression vectors and treated with alpelisib, inavolisib, or ipatasertib for 4 days. Data are normalized to vehicle-treated cells. Error bars, SD ($n = 3$). e.v., empty vector; MAF, mutant allele frequency.

this class of inhibitors (11). Therefore, when Q859 is substituted with a positively charged amino acid such as histidine or lysine (which is present at this position in PIK3Cγ), this hydrogen bonding interaction would be disrupted (Fig. 4B; Supplementary Fig. S5A and S5B). Thus, we hypothesized that Q859 mutations might specifically affect the activity of orthosteric PI3Kα-selective inhibitors.

Conversely, W780 is conserved within the ATP-binding pocket of all four PI3K isoforms (α, β, δ, or γ; Fig. 4A; ref. 12), and this amino acid physically interacts with both PI3Kα-selective inhibitors, as well as pan-PI3K inhibitors such as pictilisib (GDC-0941; Fig. 4B; Supplementary Fig. S5A). Therefore, we hypothesized that mutations at this residue could drive universal resistance to ATP-competitive PI3K inhibitors that bind the catalytic pocket.

We next conducted free energy perturbation (FEP) simulations to further predict which mutations might modify drug affinity (Supplementary Figs. S4 and S5). FEP analyses supported our structural hypotheses, predicting that the W780R mutation would decrease the affinity of the PI3Kα-selective inhibitors alpelisib and inavolisib, as well as the pan-PI3K inhibitor pictilisib and the PI3Kα/δ-selective inhibitor taselisib (GDC-0032). Conversely, FEP simulations predicted that the Q859H/K mutations would decrease the affinity of the PI3Kα-selective inhibitors alpelisib and inavolisib but would have minimal effects on the affinities of pictilisib and taselisib.

Next, to test these modeling predictions more definitively, we evaluated these hypotheses functionally by engineering the *PIK3CA*-mutant breast cancer cell lines T47D (*PIK3CA*^{H1047R}-mutant) or MCF7 (*PIK3CA*^{E545K}-mutant) to express double mutants containing the baseline *PIK3CA* mutation (H1047R or E545K) together with the emergent secondary mutation. Expression of the W780R or Q859H/K double mutants in T47D or MCF7 resulted in a significant increase in IC_{50} values for alpelisib and inavolisib, supporting the role for these acquired mutations as potential resistance mechanisms

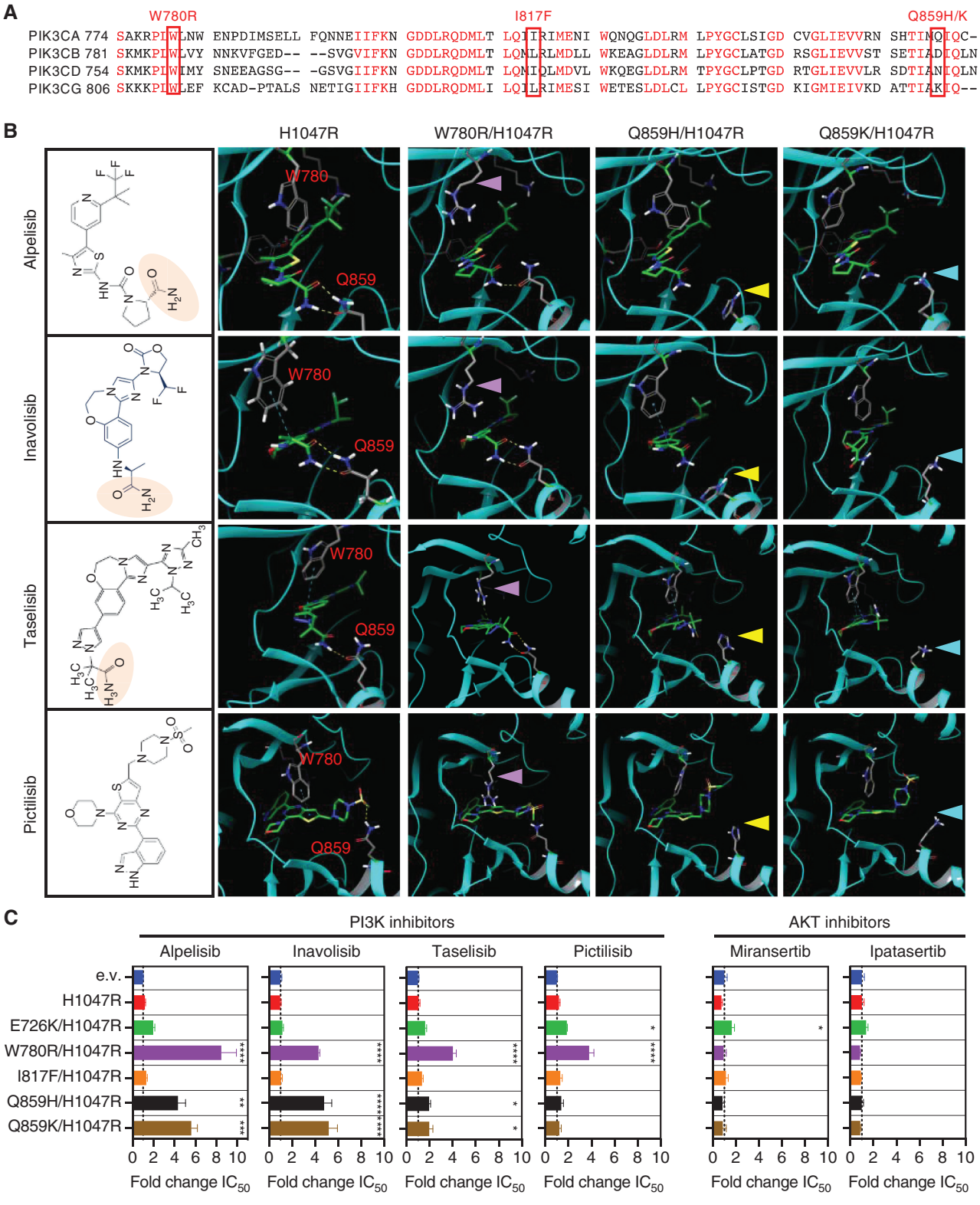

Figure 4. Mutations in *PIK3CA* involving Trp780 and Gln859 compromise the activity of orthosteric inhibitors. **A,** Amino acid sequence alignment showing the degree of conservation around the ATP binding site between the four PI3K isoforms. **B,** Chemical structures and docking analysis for alpelisib, inavolisib, taselisib, and pictilisib bound to H1047R-mutant *PIK3CA*. Amide group providing selectivity for PI3Kα is indicated with light orange shading. Colored arrowheads indicate the specified resistance mutations. **C,** Effective fold change variation resulting in 50% growth inhibitory effect is depicted for T47D cells stably infected with the indicated *PIK3CA* expression vectors. Shown is the mean and standard error ($n = 3$–4). *, $P < 0.05$; **, $P < 0.01$; ***, $P < 0.001$; ****, $P < 0.0001$; one-way ANOVA with Holm–Sidak multiple comparisons correction. (*continued on next page*)

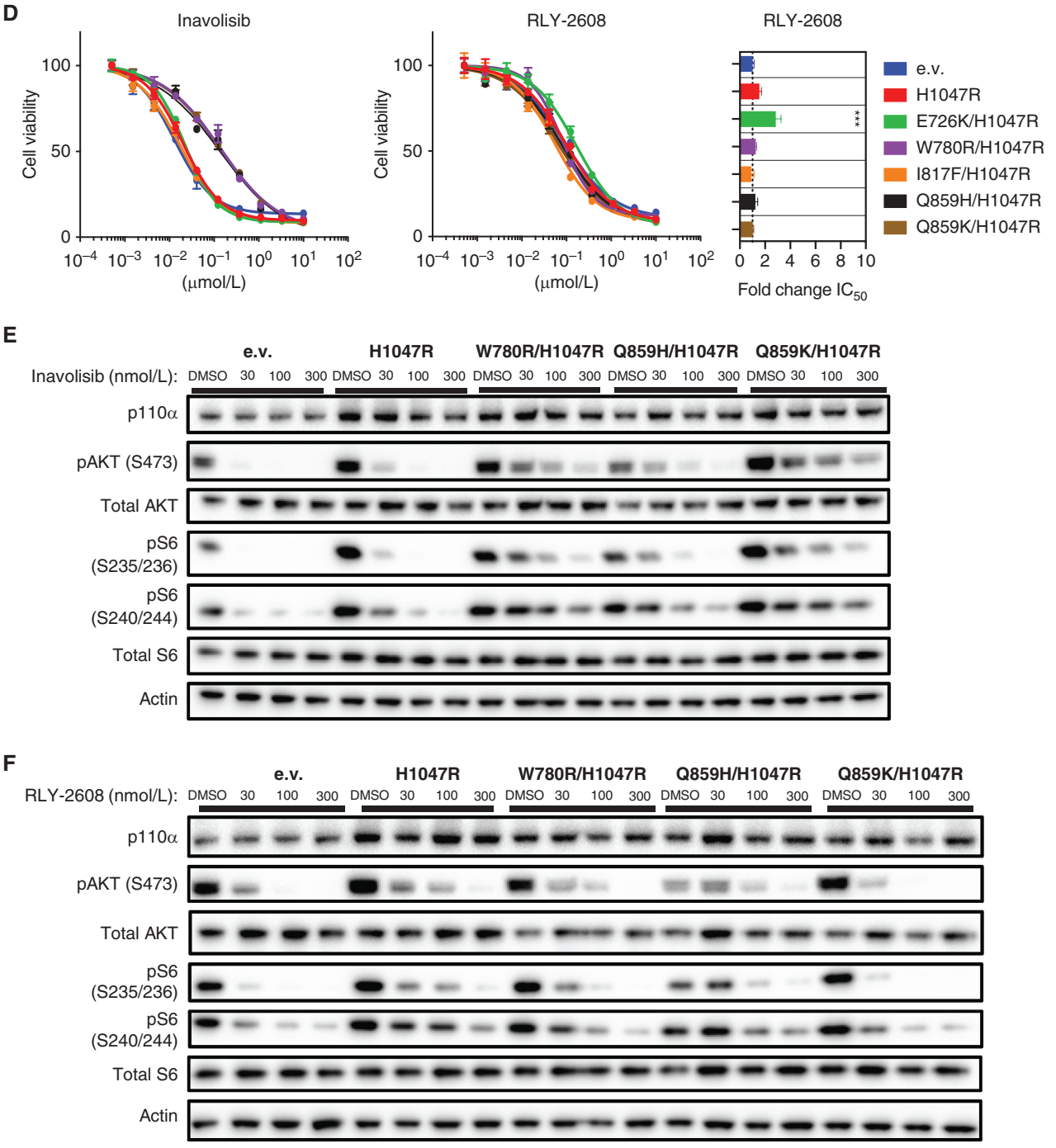

Figure 4. ***(Continued)*** **D,** Representative dose-response curves for T47D cells stably infected with the indicated *PIK3CA* expression vectors. Cell lines were treated with indicated drugs for 4 days, and cell viability was measured with CellTiter-Glo. Data are normalized to vehicle-treated cells. Error bars, SD ($n = 3$). Right, effective fold change variation resulting in a 50% growth inhibitory effect as in **C**. **E** and **F,** Western blot analysis was performed after treating T47D cells stably expressing the indicated *PIK3CA* expression vectors for 6 hours with inavolisib (**E**) or RLY-2608 (**F**). A representative blot for actin is used as a loading control. e.v., empty vector.

(Fig. 4C; Supplementary Figs. S6 and S7). Notably, we did not observe a significant change in IC_{50} in cells expressing I817F double mutants.

As predicted, W780R also led to a significant increase in IC_{50} for two additional PI3K inhibitors, pictilisib and taselisib. However, the Q859H/K mutations did not lead to a significant change in IC_{50} for the pan-PI3K pictilisib, which lacks the amide moiety present in the PI3Kα-selective inhibitors that form dual reciprocal hydrogen bonds with Q859 (Fig. 4B and C). Interestingly, the PI3Kα/δ-selective inhibitor taselisib, which also possesses an amide group, showed a mild, but significant increase in IC_{50} in the presence of the Q859H/K

mutations. Structural modeling and FEP predictions revealed that the predominant binding conformation exhibited only a single hydrogen bond (vs. dual reciprocal hydrogen bonds) with Q859, likely explaining the reduced impact of this mutation on potency (Fig. 4B; Supplementary Fig. S5). By contrast, pictilisib showed minimal hydrogen bond affinity with Q859, consistent with the lack of impact of mutations at this residue on potency.

Because these data collectively support a role for secondary *PIK3CA* mutations in acquired resistance to PI3Kα inhibitors, we focused on potential strategies to resensitize tumor cells expressing these double mutants. Therefore, we tested whether the allosteric AKT inhibitor miransertib (ARQ092) and the ATP-competitive AKT inhibitor ipatasertib, which block signaling downstream of PI3K retained efficacy in double mutant-expressing cells. We observed that both classes of AKT inhibitors were capable of restoring sensitivity in both W780R- and Q859H/K-expressing cells (Fig. 4C; Supplementary Fig. S7). Interestingly, the E726K mutation showed a modest, but significant loss of potency for pictilisib and the allosteric AKT inhibitor miransertib but did not affect the potency of other inhibitors (Fig. 4C).

Novel allosteric inhibitors that preferentially bind and inhibit mutant PI3Kα, such as H1047R, are currently in early clinical trials. RLY-2608, a first-in-class pan-mutant-selective PI3Kα inhibitor, is reported to inhibit PI3Kα harboring either kinase domain (e.g., H1047R) or helical domain (e.g., E545K) activating mutations with 7–10× selectivity over wild-type PI3Kα (Supplementary Fig. S8; ref. 13). Importantly, RLY-2608 binds to a novel allosteric pocket on PI3Kα, as opposed to the catalytic site, so we hypothesized that an inhibitor with this novel binding mode might overcome resistance in PI3Kα double mutant-expressing cells. Indeed, although W780R and Q859H/K double mutant-expressing cells show reduced sensitivity to inavolisib (Fig. 4D, left), no effect is observed on the potency of RLY-2608, relative to PI3Kα single mutant or control cells (Fig. 4D, right). Consistent with this observation, W780R and Q859H/K double mutants decreased the binding and affinity of alpelisib, but did not affect the binding of RLY-2608 (Supplementary Fig. S9).

Similarly, both inavolisib and alpelisib displayed reduced potency of downstream signaling inhibition in the presence of W780R or Q859H/K double mutants (Fig. 4E; Supplementary Figs. S10 and S11). Notably, no increases in baseline PI3K pathway activity were seen in the presence of W780R or Q859H/K double mutants. In contrast, the potency with which RLY-2608 inhibited downstream signaling was unaffected by the presence of W780R or Q859H/K double mutations (Fig. 4F; Supplementary Fig. S11A and S11B). Together, these data support a novel role for secondary *PIK3CA* mutations in clinically acquired resistance to PI3Kα orthosteric inhibitors.

DISCUSSION

PIK3CA is one of the most commonly altered oncogenes across multiple cancer lineages. Activating mutations in *PIK3CA* are found throughout the length of the p110 alpha isoform, but most are positioned within "hot-spot regions" in the helical and kinase domains. These alterations mimic and enhance to various degrees dynamic events in the natural activation process of the autoinhibited p85–p110 PI3K heterodimer, contributing to resistance to hormonal and targeted therapy (14). Alpelisib (BYL719), an orthosteric (kinase domain) PI3Kα inhibitor, is indicated for the treatment of patients with advanced *PIK3CA*-mutant breast cancer. In one of the larger cohorts of patients with acquired resistance to alpelisib and inavolisib (another orthosteric PI3Kα inhibitor) analyzed to date, we observed a diverse set of alterations expected to reactivate the PI3K/AKT pathway.

Although acquired alterations in PI3K pathway signaling nodes, such as *PTEN* loss, have previously been identified in patients with acquired resistance to PI3Kα inhibitors, our data suggest that reactivation of PI3K signaling represents a dominant mode of acquired resistance, present in nearly half of patients and involving additional classes of alterations, such as activating *AKT1* mutations and secondary *PIK3CA* mutations. Our data also show that bypass alterations outside of the PI3K pathway, such as activation of FGFR signaling or the MAPK pathway (via *KRAS* or *BRAF* alterations) are also important drivers of acquired resistance, occurring in nearly one quarter and one eighth of patients, respectively.

Our study also highlights a potentially important role for secondary *PIK3CA* mutations as a driver of acquired resistance to PI3Kα inhibitors. Notably, previous studies demonstrated that specific double *PIK3CA* mutants occurring in cis cause increased oncogenicity and sensitivity to PI3Kα inhibitors. However, our data reveal that not all secondary mutations in *PIK3CA* observed clinically have the same phenotype. In fact, some secondary mutations in *PIK3CA*, such as the W780 and Q859 mutations identified in this study, actually drive resistance to some PI3K inhibitors. We also found evidence that some *PIK3CA* double mutations, such as E726K—previously reported to increase sensitivity to PI3K inhibitors, such as alpelisib, inavolisib, and taselisib in some cancer models—may also decrease the potency of other PI3K pathway inhibitors, such as pictilisib and RLY-2608 (Fig. 4C and D). Thus, the clinical context and the specific mutation and inhibitor in question may be important factors in predicting the clinical impact of secondary *PIK3CA* mutations.

Historically, the clinical development of PI3K inhibitors has been hindered by on-target toxicity. As a result, a significant proportion of patients discontinue treatment after developing hyperglycemia, rash, or gastrointestinal adverse events. As a consequence, even a modest shift in the potency of orthosteric PI3K inhibitors driven by secondary *PIK3CA* mutations could have a significant impact on the clinical efficacy of these agents. In this study, we also show that novel allosteric PI3K inhibitors can overcome resistance driven by acquired *PIK3CA* alterations. Specifically, RLY-2608, a PI3Kα isoform-selective and pan-mutant-selective inhibitor binding to an allosteric pocket on PI3Kα, can overcome resistance mediated by secondary PI3Kα mutations within the catalytic pocket. We hypothesize that other allosteric PI3K inhibitors currently in clinical trials might also be able to overcome resistance alterations within the catalytic pocket. In addition, selective inhibition of mutant versus wild-type PI3Kα isoform minimizes the effect on insulin signaling, reducing the prevalence of hyperglycemia, and enabling higher target engagement and wider therapeutic index.

Although we identified novel secondary *PIK3CA* mutations in some patients with disease progression on PI3Kα inhibitors, our study shows that many patients develop multiple convergent resistance mechanisms reactivating oncogenic signaling through the PI3K/AKT/mTOR pathway and other bypass pathways, necessitating the development of additional rational combinations, including those between mutant-selective PI3Kα inhibitors and AKT, mTOR, or CDK inhibitors.

METHODS

Patients

Thirty-nine patients with advanced ER$^+$, HER2$^-$, breast cancer were treated with alpelisib- or inavolisib-containing regimens on clinical trials NCT01791478, NCT01872260, NCT02734615, NCT03056755, and NCT03006172. All clinical data and tumor specimens were collected and analyzed in accordance with the institutional review board–approved protocol (DFHCC 13-416), to which patients provided written informed consent, and all studies were conducted in accordance with the Declaration of Helsinki.

cfDNA Analysis

We analyzed baseline and progression targeted next-generation sequencing assays (Guardant360; Guardant Health) of 32 patients diagnosed with *PIK3CA*-mutant HR-positive, HER2-negative disease and treated with alpelisib or inavolisib. Eligibility criteria for the study included: (i) histologically confirmed diagnosis of HR-positive, HER2-negative metastatic breast cancer; (ii) documented oncogenic *PIK3CA* mutation(s) in blood or tumor per local assessment; (iii) treatment with *PIK3CA* kinase inhibitor (alpelisib or inavolisib) for more than 50 days; and (iv) matched (baseline and progression) evaluation with cfDNA assay.

Autopsy

Rapid autopsy in 8 patients (1 patient had both ctDNA analysis and autopsy performed) was performed under IRB-approved protocol DFHCC 13-416 to which patients provided written informed consent, and all studies were conducted in accordance with the Declaration of Helsinki. A standard hospital autopsy consent form was also signed by the health care proxy or next of kin, as per institutional policies. We performed WES of 100 tissue samples collected from 8 autopsy series from patients with metastatic, *PIK3CA*-mutant, HR-positive, HER2-negative breast cancer previously treated with alpelisib or inavolisib. Rapid autopsies were performed within a median of 6 hours after death. An on-call rapid autopsy team comprising a medical oncologist, an autopsy pathologist, an autopsy technician, and tissue collection coordinators performed rapid autopsies within 6 hours of the patient's death. Fresh tissue samples were snap-frozen immediately after dissection and stored at −80°C. Perimortem blood was collected for cfDNA analysis from the femoral vein or the inferior vena cava at the start of each autopsy, and blood samples were preserved in cell-free DNA BCT tubes (Streck) with subsequent plasma separation as per the manufacturer's guidelines. Separated plasma was stored at −80°C. Rapid autopsy was performed with informed consent of the healthcare proxy under IRB-approved protocol 13-416 to which patients provided written informed consent, and all studies were conducted in accordance with the Declaration of Helsinki. A standard hospital autopsy consent form was also signed by the health care proxy or next of kin, as per institutional policies.

WES Pipeline for Autopsy

WES was performed at the Broad Institute.

WES data were analyzed on the Terra cloud-based analysis platform (https:// app.terra.bio/). Somatic mutations for each tumor/normal pair were detected using the Cancer Genome Analysis (CGA) hg19 WES Characterization Pipeline available on the Terra platform. The Characterization Pipeline includes multiple steps, including MuTect (15) for the detection of somatic single-nucleotide variants, Strelka (16) for detecting small insertions and deletions (INDEL), deTiN (17) estimates potential tumor-in-normal contamination, ContEst (18) for detecting cross-patient contamination, AllelicCapSeg (19) for assessing allele-specific copy-number alterations, and ABSOLUTE (19) for estimating tumor purity, ploidy, absolute allelic copy-number and cancer cell fractions (CCF). The data for this study consisted of multiple samples collected from each patient: a pre-autopsy cfDNA sample in addition to the autopsy samples. Phylogenetic analysis, subclonal reconstruction, and tree building were done with the PhylogicNDT package (bioRxiv 2019:508127 doi 10.1101/508127).

We collected WES data from a total of 18 tumor tissue samples from across the body and 1 normal muscle tissue sample from patient 2542 at the time of autopsy. After analysis through the CGA pipeline, we identified 9 lesions with a tumor purity of greater than 15% that we could confidently use in downstream clonal analysis. We reviewed mutations and ran our extensive quality control pipeline. For phylogenetic analysis, we filtered for mutations that were present at a CCF of at least 20% in one or more samples. Finally, we ran the PhylogicNDT suite of tools and reconstructed the phylogeny of the cancer. The sequencing data have been deposited to dbGaP under the accession number phs002923.v1.p1.

Phylogenetic Analysis of Multiple Samples from the Same Patient

The PhylogicNDT algorithm (https://github.com/broadinstitute/PhylogicNDT) uses a Dirichlet process to cluster mutations based on estimated CCFs (bioRxiv 2019:508127 doi 10.1101/508127). PhylogicNDT Clustering takes in copy-number profiles, purity values, and mutation calls and uses a posterior distribution on CCFs associated with each mutation across all samples. The assignment of mutations to clusters is sampled using a Markov chain Monte-Carlo (MCMC) Gibbs sampler, which probabilistically assigns a given mutation to a new cluster or a preexisting cluster according to the multinomial probability distribution on every iteration of the algorithm. After the iterations are completed, a posterior distribution is calculated based on the resulting number of clusters and the CCF distributions of every mutation based on the average of CCF distributions on every iteration. Finally, the posterior CCF distributions for each mutation are then hierarchically clustered based on their similarities. Essentially, the mutations are clustered to maximize similarities in CCF across all lesions for the most likely clustering configuration.

The BuildTree component of PhylogicNDT uses the posterior distribution over cluster configurations and the assignment of mutations to calculate an ensemble of possible trees that support the phylogenetic relationship of the cell populations present. The algorithm uses an MCMC Gibbs sampler over the branch positions within the tree and the parent–child relationships among clones. In each iteration, a subclone can move to a place in the tree according to a multinomial probability calculated based on the pigeon-hole rule (the sum of CCFs of sibling clone cannot exceed the CCF of the parent clone), accounting for the uncertainty in assignment of mutations to subclones. The likelihood of the entire tree is determined by multiplying the pigeon-hole probabilities for all nodes in the tree (i.e., parent–child relationships). In each MCMC iteration, the tree likelihoods are used to draw the new location of a single clone. All mutations are randomly assigned to clones based on the match between their CCF distribution and the clones' CCF distributions, which are then updated based on the assignment of mutations. This mutation shuffling ensures that the uncertainty in the

tree structure also takes into account the uncertainty in mutation assignment. Finally, the MCMC generates a posterior distribution over the possible trees.

Free Energy Calculations

The reported free energy calculations were initiated from protein models based on the X-ray structure of H1047R bound to GDC-0032. The crystal structure was separately imported into the Maestro program, where all crystallographic waters were deleted, hydrogens were added to the structures to assume a pH 7 environment, and the position of the heavy atoms was locally optimized using the Protein Prep Wizard utility. This procedure optimized the protein–protein and protein–ligand hydrogen bonding and relieved unfavorable steric clashes without introducing any significant changes to the crystallographically determined positions of the heavy atoms. Once the prepared protein structure was obtained, the initial binding modes for apelisib, GDC-0077, and GDC-0941 were constructed through a standard docking protocol using Glide. Once these prepared complex structures for the compounds were obtained, free energy calculations of protein residue mutations were performed with the FEP^+ program (20) using default settings. Each λ window of the free energy calculation was simulated for a 100-ps equilibration followed by a 5-ns production simulation. To compute a meaningful binding free energy difference of the inhibitor binding to the wild-type protein versus the mutant form, the protein residue in question was alchemically mutated in the presence of the inhibitor and then again alchemically mutated in the absence of the inhibitor, with the difference in these results yielding the relative binding free energy of the inhibitor to the mutant form of the protein versus the wild-type protein.

Cell Culture and General Reagents

T47D cells were cultured in RPMI medium with 10% fetal bovine serum (FBS). MCF7 cells were cultured in DMEM/F12 medium with 10% FBS and supplemented with insulin (10 ng/mL). HEK293T cells were maintained in DMEM with 10% FBS. All cell lines were obtained from ATCC and were grown in the presence of penicillin–streptomycin at 37°C and 5% CO_2. Lentiviral particles were produced in HEK293T cells. Mutated *PIK3CA* and *AKT1* genes were introduced into T47D and MCF7 cells by lentiviral transduction followed by puromycin selection. Cell lines were obtained from ATCC and passaged for less than 6 months from receipt. Mycoplasma testing was performed routinely using a Mycoplasma PCR detection kit (ABM,#G238). All cell lines used tested negative for *Mycoplasma*.

Phospho-*AKT1* (S473) was obtained from Abcam. All the other antibodies were purchased from Cell Signaling Technology. RLY-2608 was kindly provided by Relay Therapeutics. All other compounds were purchased from MedChemExpress.

PIK3CA and *AKT1* constructs were obtained from Addgene. To generate mutants, a QuikChange II Site-Directed Mutagenesis kit (Agilent Technologies) was used. Introduced point mutations were verified by Sanger sequencing, and mutants were shuttled into a gateway-compatible pLENTI-puro vector obtained from Addgene.

Dose-Response Experiments

Viability assays were carried out using the CellTiter-Glo assay (Promega). Cells were counted and seeded in 96-well plates in triplicates. The next day, compounds were added, and 3 to 4 days later, cell viability was assessed. EC_{50} determination was performed using GraphPad Prism.

Western Blot Analysis

Cell lines were treated with alpelisib, inavolisib, or RLY-2608 for 6 hours and lysates were prepared as described previously (21). All antibodies were diluted in 5% BSA + 0.02% sodium azide in TBST as follows: p110α (1:1,000), pAKT (S473, 1:800), AKT (1:1,000), pS6 (S235/236, 1:1,500), pS6 (S240/244, 1:1,500), S6 (1:1,000), ACTIN (1:2,000).

Cell-Free DNA Extraction and ddPCR

Whole blood was collected by routine phlebotomy in two 10-mL Streck tubes. Plasma was separated within 1 to 4 days of collection through two different centrifugation steps (the first at room temperature for 10 minutes at 1,600 × *g* and the second at 3,000 × *g* for the same time and temperature). Plasma was stored at −80°C until cfDNA extraction. cfDNA was extracted from plasma using the QIAamp Circulating Nucleic Acid Kit (QIAGEN) with 60 minutes of proteinase K incubation at 60°C. All other steps were performed according to the manufacturer's instructions. For ddPCR experiments, DNA template (up to 10 μL, with a total of 20 ng for each specimen) was added to 10 μL ddPCR Supermix for Probes (Bio-Rad) and 2 μL custom primer/probe mixture. This reaction mix was added to a DG8 cartridge together with 60 μL Droplet Generation Oil for Probes (Bio-Rad) and used for droplet generation. Droplets were then transferred to a 96-well plate (Eppendorf) and then thermal cycled with the following conditions: 10 minutes at 95°C, 40 cycles at 94°C for 30 seconds, 55°C (with a few grades of difference among assays) for 1 minute, followed by 98°C for 10 minutes (Ramp Rate 2°C/s). Droplets were analyzed with the QX200 Droplet Reader (Bio-Rad) for fluorescent measurement of FAM and HEX probes. Gating was performed based on positive and negative controls, and mutant populations were identified. The ddPCR data were analyzed with QuantaSoft analysis software (Bio-Rad) to obtain a fractional abundance of the mutant DNA alleles in the wild-type/normal background. The quantification of the target molecule was presented as the number of total copies (mutant plus wild-type) per sample in each reaction. An allelic fraction was calculated as follows: AF % = [Nmut/(Nmut + Nwt) × 100], where Nmut is the number of mutant alleles and Nwt is the number of wild-type alleles per reaction. ddPCR analysis of normal control plasma DNA and no DNA template controls was always included. Probe and primer sequences are available upon request.

Surface Plasmon Resonance Binding Assay

Recombinant PI3Ka enzymes were immobilized onto a biosensor surface via amine coupling, prior to compound injection onto the protein-immobilized surface, using a Biacore S200 (Cytiva Lifesciences). The resulting binding data generated at 37°C were fit kinetically to a 1:1 binding model to calculate binding rates and affinities.

Data Availability

The breakdown of acquired genomic PI3K alterations found in clinical cfDNA assays at progression to orthosteric *PIK3CA* inhibitors is shown in Supplementary Table S3. WES data from autopsies are deposited at dbGaP under the accession number phs002923.v1.p1. PCR probes are shown in Supplementary Figs. S2 and S6, and are available through direct communication with the corresponding author.

Authors' Disclosures

A. Varkaris reports a clinical trial contract for Mass General Cancer Center with Relay Therapeutics, Beigene, and Boehringer Ingelheim. I. Leshchiner reports personal fees, nonfinancial support, and other support from ennov1, LLC, and NoRD Bio, Inc., and personal fees and nonfinancial support from PACT Pharma, Inc., during the conduct of the study. G.M. Wulf reports grants 5R01CA226776-05 and 22-177 from the NIH and Breast Cancer Research Foundation (BCRF) respectively during the conduct of the study and other support from Glaxo Smith Kline, Genentech, Gilead, and Seagen outside the submitted work; in addition, G.M. Wulf has a patent for US 20090258352 A1 issued, licensed, and with royalties paid from R&D Systems, Cell

Signaling Technology. A. Bardia reports grants and personal fees from Pfizer, Novartis, Genentech, Merck, Radius Health/Menarini, Immunomedics/Gilead, Sanofi, Daiichi Pharma/Astra Zeneca, Eli Lilly, and Foundation Medicine during the conduct of the study. L.M. Spring is a consultant for/on the advisory board of Novartis, Puma, G1 Therapeutics, Daiichi Pharma, Astra Zeneca, and Eli Lilly and reports institutional research support from Merck, Genentech, Gilead, and Eli Lilly. E. Pazolli reports other support from Relay Therapeutics during the conduct of the study and outside the submitted work. G. Getz reports grants from IBM, Pharmacyclics, and Ultima Genomics during the conduct of the study; personal fees and other support from Scorpion Therapeutics outside the submitted work; is an inventor on patent applications related to MSMuTect, MSMutSig, MSIDetect, Polysolver, SignatureAnalyzer-GPU and MinimuMM-seq; and is a founder and consultant and holds privately held equity in Scorpion Therapeutics. R.B. Corcoran reports personal fees and other support from Alterome Therapeutics, Sidewinder Therapeutics, other support from Erasca, Kinnate, Revolution Medicines, Cogent Biosciences, C4 Therapeutics, Nested Therapeutics, Remix Therapeutics, Interline Therapeutics, nRichDx, other support from Avidity Biosciences, grants and personal fees from Pfizer, personal fees from AbbVie, Asana Biosciences, Elicio, FOG Pharma, Guardant Health, Mirati Therapeutics, Natera, Qiagen, Taiho, and grants from Lilly, Novartis, and Invitae outside the submitted work. D. Juric reports grants and personal fees from Astra Zeneca, Pfizer, Syros, Roche, Eli Lilly, Eisai, Genentech, personal fees from Guardant Health, Ipsen, Novartis, personal fees and other support from PIC Therapeutics, Relay Therapeutics, grants and personal fees from Syros, personal fees from Vibliome, Transcode, grants from Arvinas, Blueprint Medicines, InventisBio, Ribon Therapeutics, Scorpion Therapeutics, Seagen, and Takeda outside the submitted work. No disclosures were reported by the other authors.

Authors' Contributions

A. Varkaris: Formal analysis, supervision, investigation, writing–original draft, project administration, writing–review and editing. **F. Fece de la Cruz:** Conceptualization, investigation, writing–original draft, writing–review and editing. **E.E. Martin:** Conceptualization, data curation, writing–original draft. **B.L. Norden:** Formal analysis, investigation, methodology. **N. Chevalier:** Data curation, investigation. **A.M. Kehlmann:** Resources, data curation. **I. Leshchiner:** Data curation, formal analysis, supervision. **H. Barnes:** Data curation, formal analysis. **S. Ehnstrom:** Data curation, formal analysis. **A.-M. Stavridi:** Formal analysis, investigation. **X. Yuan:** Data curation, investigation. **J.S. Kim:** Investigation. **H. Ellis:** Investigation. **A. Papatheodoridi:** Data curation, investigation. **H. Gunaydin:** Data curation, investigation. **B.P. Danysh:** Data curation, project administration. **L. Parida:** Data curation, software. **I. Sanidas:** Investigation. **Y. Ji:** Investigation. **K. Lau:** Investigation. **G.M. Wulf:** Investigation. **A. Bardia:** Investigation. **L.M. Spring:** Investigation. **S.J. Isakoff:** Investigation. **J.K. Lennerz:** Data curation, investigation. **L. Pierce:** Data curation, formal analysis. **E. Pazolli:** Data curation, investigation, methodology. **G. Getz:** Conceptualization, resources, data curation, supervision, funding acquisition. **R.B. Corcoran:** Conceptualization, resources, supervision, funding acquisition, investigation, writing–original draft, writing–review and editing. **D. Juric:** Conceptualization, resources, formal analysis, supervision, funding acquisition, investigation, methodology, writing–original draft, writing–review and editing.

Acknowledgments

This work was supported by Department of Defense Physician Research Award (PC200820) and ASCO YIA (to A. Varkaris), NIH (R37 CA225655) to J.K. Lennerz, NIH RO1 CA226776 (to G.M. Wulf), NIH/NCI Moonshot DRSN U54CA224068 (to R.B. Corcoran), and Susan Eid Tumor Heterogeneity Initiative (to D. Juric).

The publication costs of this article were defrayed in part by the payment of publication fees. Therefore, and solely to indicate this fact, this article is hereby marked "advertisement" in accordance with 18 USC section 1734.

Note

Supplementary data for this article are available at Cancer Discovery Online (http://cancerdiscovery.aacrjournals.org/).

Received June 20, 2023; revised September 20, 2023; accepted October 23, 2023; published first October 31, 2023.

REFERENCES

1. Andre F, Ciruelos E, Rubovszky G, Campone M, Loibl S, Rugo HS, et al. Alpelisib for PIK3CA-mutated, hormone receptor-positive advanced breast cancer. N Engl J Med 2019;380:1929–40.
2. Juric D, Castel P, Griffith M, Griffith OL, Won HH, Ellis H, et al. Convergent loss of PTEN leads to clinical resistance to a PI(3)Kalpha inhibitor. Nature 2015;518:240–4.
3. Hopkins BD, Pauli C, Du X, Wang DG, Li X, Wu D, et al. Suppression of insulin feedback enhances the efficacy of PI3K inhibitors. Nature 2018;560:499–503.
4. Razavi P, Dickler MN, Shah PD, Toy W, Brown DN, Won HH, et al. Alterations in PTEN and ESR1 promote clinical resistance to alpelisib plus aromatase inhibitors. Nat Cancer 2020;1:382–93.
5. Savas P, Lo LL, Luen SJ, Blackley EF, Callahan J, Moodie K, et al. Alpelisib monotherapy for PI3K-altered, pretreated advanced breast cancer: A Phase II Study. Cancer Discov 2022;12:2058–73.
6. Bertucci A, Bertucci F, Goncalves A. Phosphoinositide 3-Kinase (PI3K) inhibitors and breast cancer: an overview of current achievements. Cancers (Basel) 2023;15:1416.
7. Carpten JD, Faber AL, Horn C, Donoho GP, Briggs SL, Robbins CM, et al. A transforming mutation in the pleckstrin homology domain of AKT1 in cancer. Nature 2007;448:439–44.
8. Yi KH, Axtmayer J, Gustin JP, Rajpurohit A, Lauring J. Functional analysis of non-hotspot AKT1 mutants found in human breast cancers identifies novel driver mutations: implications for personalized medicine. Oncotarget 2013;4:29–34.
9. Vanhaesebroeck B, Perry MWD, Brown JR, Andre F, Okkenhaug K. PI3K inhibitors are finally coming of age. Nat Rev Drug Discov 2021;20:741–69.
10. Zheng Z, Amran SI, Thompson PE, Jennings IG. Isoform-selective inhibition of phosphoinositide 3-kinase: identification of a new region of nonconserved amino acids critical for p110alpha inhibition. Mol Pharmacol 2011;80:657–64.
11. Zhang M, Jang H, Nussinov R. PI3K inhibitors: review and new strategies. Chem Sci 2020;11:5855–65.
12. Corpet F. Multiple sequence alignment with hierarchical clustering. Nucleic Acids Res 1988;16:10881–90.
13. Pazolli E, Kipp R, B A, Gunaydin H, Iskandar A, Zubrowski M, et al. Discovery and characterization of RLY-2608: The first allosteric, mutant, and isoform-selective inhibitor of PI3Kα. Mol Cancer Ther 2021;20(12 Suppl):P251.
14. Burke JE, Perisic O, Masson GR, Vadas O, Williams RL. Oncogenic mutations mimic and enhance dynamic events in the natural activation of phosphoinositide 3-kinase p110alpha (PIK3CA). Proc Natl Acad Sci U S A 2012;109:15259–64.
15. Cibulskis K, Lawrence MS, Carter SL, Sivachenko A, Jaffe D, Sougnez C, et al. Sensitive detection of somatic point mutations in impure and heterogeneous cancer samples. Nat Biotechnol 2013;31:213–9.
16. Saunders CT, Wong WS, Swamy S, Becq J, Murray LJ, Cheetham RK. Strelka: accurate somatic small-variant calling from sequenced tumor-normal sample pairs. Bioinformatics 2012;28:1811–7.
17. Taylor-Weiner A, Stewart C, Giordano T, Miller M, Rosenberg M, Macbeth A, et al. DeTiN: overcoming tumor-in-normal contamination. Nat Methods 2018;15:531–4.

18. Cibulskis K, McKenna A, Fennell T, Banks E, DePristo M, Getz G. ContEst: estimating cross-contamination of human samples in next-generation sequencing data. Bioinformatics 2011;27:2601–2.
19. Carter SL, Cibulskis K, Helman E, McKenna A, Shen H, Zack T, et al. Absolute quantification of somatic DNA alterations in human cancer. Nat Biotechnol 2012;30:413–21.
20. Steinbrecher T, Abel R, Clark A, Friesner R. Free energy perturbation calculations of the thermodynamics of protein side-chain mutations. J Mol Biol 2017;429:923–9.
21. Ahronian LG, Sennott EM, Van Allen EM, Wagle N, Kwak EL, Faris JE, et al. Clinical acquired resistance to RAF inhibitor combinations in BRAF-mutant colorectal cancer through MAPK pathway alterations. Cancer Discov 2015;5:358–67.